# RSC Advances

ROYAL SOCIETY OF CHEMISTRY

www.rsc.org/advances

RSC Advances RSCPublishing

PAPER

Cite this: DOI: 10.1039/x0xx00000x

Received 00th January 2012,
Accepted 00th January 2012

DOI: 10.1039/x0xx00000x

www.rsc.org/

# Bimetallic Pt-Ni composites on ceria-doped alumina supports as catalysts in the aqueous-phase reforming of glycerol

M. M. Rahman,* Tamara L. Church, Meherzad F. Variava, Andrew T. Harris, and Andrew I. Minett*[a]

Although Pt is the most appropriate catalyst for aqueous phase reforming (APR) of glycerol to generate $H_2$, it is expensive. We studied its possible minimization to levels where acceptable $H_2$ yields are still maintained. When an additional catalytic metal, Ni, was introduced to our Pt/$CeO_2$–$Al_2O_3$ catalyst, the Pt content could be reduced from 3 to 1 wt%, with a slight increase in $H_2$ production. In this study, Pt and Ni in various ratios were supported on alumina doped with 3 wt% ceria, and the resulting materials were characterized and tested as catalysts for the APR of glycerol. Amongst the catalysts tested, bimetallic 1Pt-6Ni/3CeAl (containing 1 wt% Pt and 6 wt% Ni) gave the highest $H_2$ yield (86%) and gas-phase C yield (94%). Thus, although 1Pt-6Ni/3CeAl and our reported 3Pt/3CeAl catalyst produced almost same amount of $H_2$ (1.8 and 1.9 mmol, respectively) per gram of catalyst per hour, the latter produced three times as much $H_2$ per gram of Pt per hour (195 mmol); this measure is crucial to the competitiveness of a catalyst in large-scale $H_2$ production. X-ray diffraction (XRD) patterns and thermogravimetric analyses of the spent catalysts showed no serious catalyst deactivation by carbon deposition after 30 h on stream, except in the case of Pt-free 6Ni/3CeAl, which ceased to produce $H_2$ after 15 h on stream. XRD and X-ray photoelectron spectroscopic analyses demonstrated that adding Ni impacted both the crystallite and electronic structure of Pt. These effects likely conspired to produce the high glycerol conversion and gas phase C yield and, ultimately, the high $H_2$ yield observed over 1Pt-6Ni/3CeAl.

## Introduction

Although hydrogen ($H_2$) has the potential to become an environmentally friendly energy carrier because of its high energy density and lack of carbonaceous combustion products, its use is currently problematic in that 95% of $H_2$ is produced from fossil fuels.[1] Therefore, considerable research has focused on producing $H_2$ from renewable sources.[2] Dumesic and co-workers pioneered the catalytic aqueous phase reforming (APR) of polyols (which can be derived from biomass) under relatively mild reaction conditions (200–250 °C, 20–50 bar) to produce a hydrogen-rich gas[3, 4] that contains less CO (<300 ppm) than the product stream from conventional steam reforming does.[5] Studies examining kinetics[6] and catalyst design[3, 7, 8] have demonstrated that APR (decomposition into CO and $H_2$ is shown in Eq. 1 for the case of glycerol) involves the cleavage of C–C and C–H bonds to form metal-bound surface species, especially CO, which can then react with $H_2O$ to form $H_2$ and $CO_2$ via the water–gas shift (WGS) reaction (Eq. 2). The overall APR of a mole of glycerol (Eq. 3) produces a maximum of seven moles of hydrogen (four from the reforming reaction and three from the WGS reaction). Thus, a good APR catalyst must catalyze both C–C bond cleavage and the WGS reaction[9] without promoting competing reactions such as C–O cleavage or methanation (Eq. 4), which can greatly deteriorate the yield of $H_2$. Group VIII metals, particularly Pt, Pd and Ni, are especially effective.[10]

$$C_3H_8O_3 \rightleftharpoons 3\ CO + 4\ H_2 \qquad (1)$$

$$3\ CO + 3\ H_2O \rightleftharpoons 3\ CO_2 + 3\ H_2 \qquad (2)$$

$$C_3H_8O_3 + 3\ H_2O \rightleftharpoons 3\ CO_2 + 7\ H_2 \qquad (3)$$

$$4\ H_2 + CO_2 \rightleftharpoons CH_4 + 2\ H_2O \qquad (4)$$

We recently reported that Pt supported on alumina doped with 3 wt% ceria gave significantly higher $H_2$ yield and selectivity from the APR of glycerol than Pt on alumina.[11] The improved performance of these catalysts was attributed to their higher coking resistance and oxygen storage capacity, as well as to enhanced catalysis of the WGS reaction and lower methanation activity under APR conditions. Although Pt catalysts are highly active for APR,[9] the high cost of Pt makes catalysts based on non-precious metals desirable. Ni has shown initial APR activity comparable to that of Pt, but was subject to significant deactivation.[10] Thus, efforts have been made to improve the catalytic activities of Ni catalysts by impregnating them with other metallic elements.[12]

The activity of APR catalysts, as well as of other supported-metal catalysts, can be enhanced by adding an additional metal. It has been suggested that adding noble metal promoters to a Ni catalyst for dry methane reforming may reduce coke deposition and therefore provide stability.[13] Relevant to C–C bond cleavage, adding Pd to a Ni/$SiO_2$ catalyst increased the amount of gas produced from cellulose pyrolysis; this was attributed to greater tar-cracking activity.[14] The Pt-Ni system in particular has been extensively studied in a range of applications because of its synergetic catalytic effect.[15] Kunkes et al. reported the conversion of glycerol by APR over carbon-supported Pt (5 wt%) and Pt-Re catalysts. The addition of Re led to an increase in the production of $H_2$, CO, $CO_2$, and light alkanes (primarily methane) and, ultimately, to better hydrogen selectivity.[16] Wang et al. showed that adding Co to a Pt-based (8 wt%) APR catalyst significantly increased its activity without impacting the selectivity for $H_2$.[17] Manfro et al.[18] added Cu to a Ni catalyst and obtained decreased $CH_4$ formation, which increased $H_2$ selectivity. Ko et al.[19] showed that, under the same pretreatment conditions, Pt-Ni bimetallic catalysts had more active sites than monometallic Pt or Ni catalysts. Tupy et al.[20] found that, after 24 h on-stream in the APR of ethylene glycol, a supported Pt-Ni (2.7 wt%) catalyst was more active than a Pt catalyst with the same Pt content because Ni segregation occurred, producing a Ni-enriched surface. Huber et al.[5] suggested that the activity of Pt-based (3 wt%) catalysts for APR could be increased by alloying Pt with Ni or Co, which would decrease the strength with which CO and $H_2$ interact with the surface, thereby increasing the fraction of catalytic sites available to react with ethylene glycol. Therefore, we investigated the addition of Ni to our Pt catalysts supported on 3-wt%-ceria-doped alumina. The ratio of Pt to Ni on the support was optimized and the catalyst characterized to better understand the system.

## Results and discussion

### Structural Characteristics of Synthesized Catalysts

The textural properties of the catalysts and supports were evaluated from nitrogen adsorption-desorption isotherms at –196 °C, and the results are shown in Figure S1 and summarized in Table 1. The support, composed of 3 wt% $CeO_2$ in $Al_2O_3$, had $S_{BET}$ = 162 $m^2\ g^{-1}$.[11] Adding 6 wt% Ni lowered the surface area to 125 $m^2\ g^{-1}$, whereas adding Pt (1 or 3 wt%) caused a smaller loss of surface area, to ~150 $m^2\ g^{-1}$.[11] As Ni was added to 1Pt/3CeAl, $S_{BET}$ and $V_p$ gradually decreased. $D_p$ decreased significantly when 12 or 18 wt% Ni was present.

**Table 1.** Textural properties of catalysts.[a]

| Supports/ Catalysts | $S_{BET}$ | $V_P$ | $D_P$ | Particle size | | $M_{disp}$ |
|---|---|---|---|---|---|---|
| | | | | Ni | Pt | |
| | ($m^2\ g^{-1}$)[b] | ($cm^3\ g^{-1}$)[c] | (nm)[d] | (nm)[e] | (nm)[e] | (%)[f] |
| $3CeO_2–Al_2O_3$ (3CeAl) | 162 | 0.28 | 4.9 | NA[g] | NA[g] | NA[g] |
| 1Pt/3CeAl | 149 | 0.25 | 4.8 | NA[g] | 11 | 10 |
| 6Ni/3CeAl | 125 | 0.22 | 4.9 | –[h] | NA[g] | NA[g] |
| 1Pt-3Ni/3CeAl | 139 | 0.23 | 4.9 | –[h] | 8.8 | 13 |
| 1Pt-6Ni/3CeAl | 120 | 0.20 | 4.9 | –[h] | 4.6 | 25 |
| 1Pt-12Ni/3CeAl | 116 | 0.19 | 4.3 | 12 | 8.1 | 14 |
| 1Pt-18Ni/3CeAl | 109 | 0.18 | 4.3 | 21 | 6.7 | 17 |

[a] Measured by $N_2$ adsorption/desorption at –196 °C. Prior to measurement, samples were calcined in air at 600 °C for 6 h. [b] Specific surface area ($S_{BET}$) was determined from the linear portion of the isotherm ($P/P_0$ = 0.05–0.35).[21] [c] Pore volume ($V_p$) was calculated at $P/P_0$ = 0.995. [d] Predominant pore size ($D_p$, volume basis) was calculated from the adsorption isotherm using the Barrett–Joyner–Halenda (BJH) formula.[22] [e] Calculated by applying the Scherrer equation[23] to the XRD peak generated from the (200) plane of Ni or the (111) plane of Pt in the reduced catalysts (Figure 2). [f] $M_{disp}$ = metal dispersion of Pt and Pt-Ni, calculated according to Eq. 5.[24] [g] Not applicable. [h] Peak was too small and broad to be measured reliably.

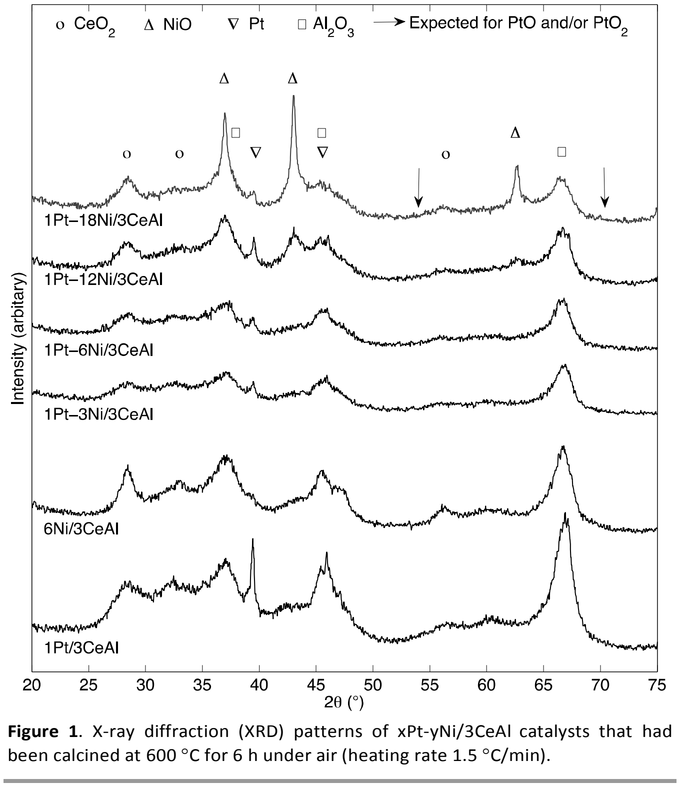

**Figure 1**. X-ray diffraction (XRD) patterns of xPt-yNi/3CeAl catalysts that had been calcined at 600 °C for 6 h under air (heating rate 1.5 °C/min).

The XRD patterns of the catalysts after calcination and reduction are shown in Figures 1 and 2, respectively. As expected, the characteristic peaks of NiO in the patterns of the calcined catalysts intensified and became sharper as the Ni content increased from 3 to 18 wt%, indicating that both the relative amount of crystalline NiO and its crystallite size increased with increasing Ni content. At higher Ni loading (≥12 wt%), three clear diffraction lines of the NiO fluorite structure were observed at 2θ = 37.2, 43.3, and 62.9°, representing the (111), (200), and (220) planes, respectively;[25, 26] the last one in particular was difficult to discern at lower Ni loadings. Two clear diffraction peaks representing the (111) and (200) planes, respectively, of metallic platinum[27] were observed at 2θ = 39.9 and 45.9°. Neither PtO (JCPDS 43-1100) nor $PtO_2$ (JCPDS 23-1306) were present in significant amounts. Three broad peaks at 2θ = 38, 46, and 67° in the XRD pattern indicated the presence of $\gamma$-$Al_2O_3$,[28] and those at 2θ = 29, 33, and 56° represented the fluorite-structured $CeO_2$.[29]

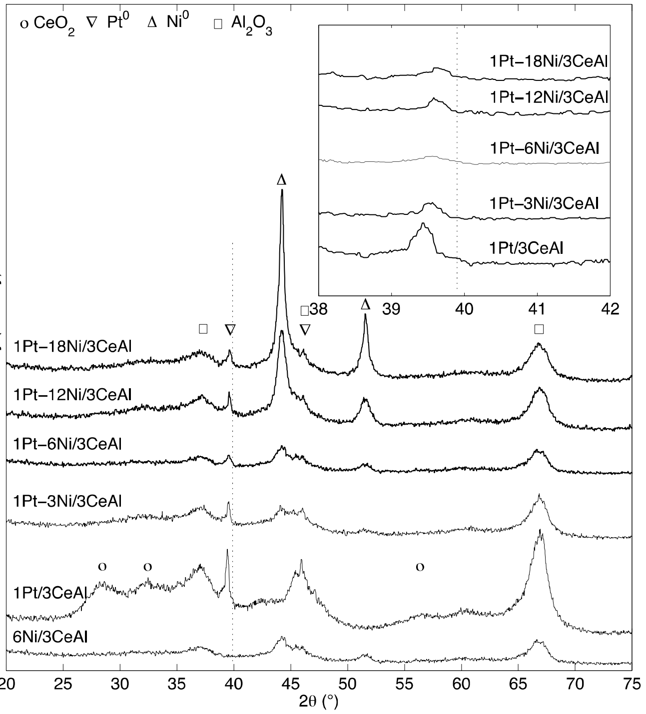

**Figure 2.** X-ray diffraction patterns of catalysts that had been reduced in flowing $H_2$ (50 vol.% in $N_2$) at 800 °C for 60 min (heating rate 1.5 °C $min^{-1}$). 1Pt/3CeAl was reduced at 500 °C. Inset shows the Pt (111) peak region.

Figure 2 shows the XRD patterns of the catalysts following reduction at 800 °C. These demonstrated that NiO was completely reduced to $Ni^0$, with diffraction peaks at 2θ = 44.5 and 51.8° corresponding to the (111) and (200) planes, respectively.[25] The peak intensities, and thus the amount of detectable crystalline $Ni^0$, increased with increasing Ni content. The $Ni^0$ crystallite sizes for 1Pt-12Ni/3CeAl and 1Pt-18Ni/3CeAl were calculated based upon the peak at 51.8°, and were larger on the latter sample (see Table 1). The $Ni^0$ peaks in the XRD patterns of the remaining catalysts were not sufficiently intense to permit reliable calculations of particle size, but were qualitatively broad, suggesting smaller metal particles. The diffraction peak representing the Pt (111) reflection occurred at higher 2θ in all Pt-Ni samples than in monometallic 1Pt/3CeAl, as shown in Figure 2 (inset). This type of peak shift, which has also been observed by Tegou et al. for Pt-Ni particles (Pt/Ni ~ 4)[30] and by Fu et al.[31] for Ni@Pt core-shell nanoparticles at high Ni/Pt ratios, can indicate the formation of a solid solution, i.e., an alloy. Two thermodynamic alloys of these metals, NiPt and $Ni_3Pt$, are known, and can be produced in ordered form at 645 and ~580 °C, respectively;[32] thus both could have formed under the catalyst-reduction conditions used here. Diffraction peaks at 2θ = 41.1 or 41.6° have been assigned to the (111) reflection of NiPt;[33,34] whereas a peak at 2θ = 40.1° has been assigned to $Ni_3Pt$.[34] Though neither of these alloys appeared as bulk phases in any of our samples (see Figure 2, inset), near-surface alloys of Ni and Pt may have produced the observed shift in 2θ for Pt (111),[30] and would be expected to impact the reactivity of the metal.[35-37]

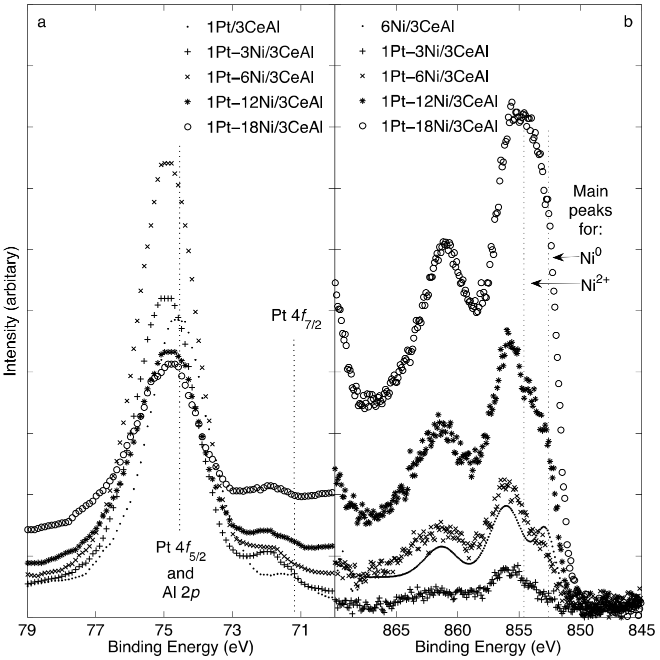

**Figure 3** The Pt 4*f* and Al 2*p* region of the X-ray photoelectron spectra of xPt-yNi/3CeAl catalysts that had been reduced in flowing $H_2$ (50 vol.% in $N_2$) at 800 °C for 60 min (heating rate 1.5 °C $min^{-1}$). 1Pt/3CeAl was reduced at 500 °C.

In addition to a shift in its position, the Pt (111) peak varied in breadth among the XRD patterns of our supported Pt–Ni materials. The mean diameter of the Pt (or Pt-Ni) crystallites was calculated by applying the Scherrer equation to this peak, and the results are shown in Table 1, together with the corresponding Pt (or Pt-Ni) dispersions. Notably, all of the bimetallic Pt-Ni catalysts bore smaller crystallites than the monometallic Pt catalyst with the same Pt loading; thus, adding Ni to the catalysts reduced the crystallite size from 11 nm for 1Pt/3CeAl to as low as 4.6 nm for 1Pt-6Ni/3CeAl. Larger amounts of Ni (12 and 18 wt%) did not promote further reduction in Pt-Ni crystallite sizes. As the catalyst with 1 wt% Pt and 6 wt% Ni showed the greatest peak width at half height for Pt (111), it had the greatest calculated metal dispersion ($M_{disp}$ = 25%, Table 1). Auspiciously, this value was significantly higher than that for the Pt-only catalyst ($M_{disp}$ = 10%). Even in the case that these Pt particles contained dissolved Ni atoms, Pt atoms are expected to form the surface layer of a solid solution of Ni in Pt that is produced under $H_2$,[35] so greater dispersion implies that a greater fraction of the Pt atoms in the sample existed on the particle surfaces.

As shown in Figure 3a, the Pt $4f_{7/2}$ XPS peaks of Pt-Ni catalysts occurred at higher binding energies than that of 1Pt/3CeAl; thus, the electronic environment of Pt was modified when Ni was introduced. A similar effect has been observed in the X-ray photoelectron spectra of core-shell Pt-coated Au nanoparticles.[38] On the other hand, nanoparticles of Pt/Ni alloys have actually shown lower Pt $4f_{7/2}$ binding energies than Pt nanoparticles synthesized according to the same methods.[31, 34] Among our 1Pt-yNi/3CeAl samples, Ni addition had the greatest impact on the Pt $4f_{7/2}$ binding energy in 1Pt-3Ni/3CeAl and 1Pt-6Ni/3CeAl ($BE_{Pt\ 4f(7/2)}$ = 71.29 and 71.35 eV, respectively; cf. 71.09 eV for 1Pt/3CeAl), suggesting that the electronic impacts of Ni–Pt interactions were most significant in those samples. The Ni $2p_{3/2}$ regions of the XPS spectra also varied among catalysts (Figure 3b). Although the impact of Pt:Ni ratio on the Ni $2p_{3/2}$ XPS regions of alloyed Pt/Ni particles has been studied quantitatively,[34] the lower concentrations of Ni on our supported catalysts did not produce XPS signals of sufficient quality for quantitative analysis. However, both $Ni^0$ (main peak at 852.6 eV[39]) and $Ni^{2+}$ (main peak at 854.6 eV,[39] present as $Ni(OH)_2$ and possibly also as NiO) were clearly visible in the spectra of all Ni-containing catalysts except 1Pt-3Ni/CeAl, albeit in varying relative amounts. The nickel hydroxides and oxides likely formed on the surface of the $Ni^0$ particles upon air exposure of the reduced catalyst prior to analysis. Although we cannot exclude the possibility that some $Ni^{2+}$ remained following the treatment in $H_2$, neither NiO nor $Ni(OH)_2$ (JCPDS 14-0117) were evident in the XRD patterns of the reduced catalysts, supporting the notion that they were minor contaminants. The Ni $2p_{3/2}$ signal in the X-ray photoelectron spectrum of 1Pt-3Ni/3CeAl was too weak to be interpreted reliably. In the future, EXAFS or XANES studies may shed further light on the nature of the interactions between Ni and Pt on $CeO_2–Al_2O_3$ supports;[20, 40] however, it is clear from the XRD and XPS evidence that adding Ni impacted both the electronic and crystallite structure of Pt. Further, energy-dispersive spectroscopic (EDS) analysis of 1Pt-18Ni/3CeAl confirmed that Ni and Pt co-existed in some areas on that material (Figure S8).

### Catalytic tests

An aqueous solution of 1 wt% glycerol was used to evaluate the performance of the catalysts. All reactions were performed using the optimised reaction conditions determined for our 3Pt/3CeAl catalyst,[11] i.e. at 240 °C, 40 bar, and with a feed flow rate of 0.05 mL $min^{-1}$, irrespective of the catalyst used. The reaction data presented in Figures 4 and 5 show that the aqueous-phase reforming of glycerol over any of the studied catalysts indeed led to a hydrogen-rich gas phase. Alkanes larger than methane (i.e. ethane) were only detected in trace amounts and were not quantified. No CO was detected, indicating that CO concentration in the product gas was below the GC detection limit (i.e. [CO] ≤ 100 ppm) in all reactions.

The $H_2$ yields (Figure 4) and concentrations in the gaseous products (Figure 5) from glycerol reforming over three of the nickel-containing catalysts, 1Pt-6Ni/3CeAl, 1Pt-12Ni/3CeAl and 1Pt-18Ni/3CeAl, were similar to those obtained over our reported 3Pt/3CeAl catalyst ($H_2$ yield = 78%; $[H_2]$ in the gaseous products = 69%),[11] despite that these catalysts contained one third as much Pt. Among these three best nickel-containing catalysts, the $H_2$ yield decreased with increasing Ni loading. Thus the highest $H_2$ yield (86%) and selectivity (83%) were observed for APR over 1Pt-6Ni/3CeAl. The lowest $H_2$ yield (13%) and $H_2$ selectivity (57%) among any of the catalysts was observed over Pt-free 6Ni/3CeAl. The $H_2$ selectivity obtained from 1Pt-6Ni/3CeAl was quite similar to those reported by Lehnert and Claus[41] for 3 wt% Pt catalysts supported on alumina (highest $H_2$ selectivity, 85%, obtained at 250 °C/20 bar, 10 wt% glycerol flowing at 0.5 mL $min^{-1}$) and by Cortright et al.[3] for 3 wt% Pt catalysts supported on nanofibers of γ-alumina (highest $H_2$ selectivity was 75%, obtained at 225 °C/29 bar, 10 wt% glycerol flowing at 0.06 mL $min^{-1}$). Moreover, the APR of glycerol over 1Pt-6Ni/3CeAl, 1Pt-12Ni/3CeAl and 1Pt-18Ni/3CeAl produced higher $H_2$ selectivity than that over the C-supported Pt and Pt-Re catalysts reported by King et al.,[42] who obtained 56% selectivity for $H_2$ when flowing a 10-wt% glycerol solution through 200 mg catalyst at 225 °C and 30 bar. Notably, the APR of glycerol over 1Pt-6Ni/3CeAl, 1Pt-12Ni/3CeAl and 1Pt-18Ni/3CeAl produced more $CO_2$ than that over 1Pt/3CeAl (Figure 4), or even 3Pt/3CeAl, which produced 62% $CO_2$ yield.[11] This is

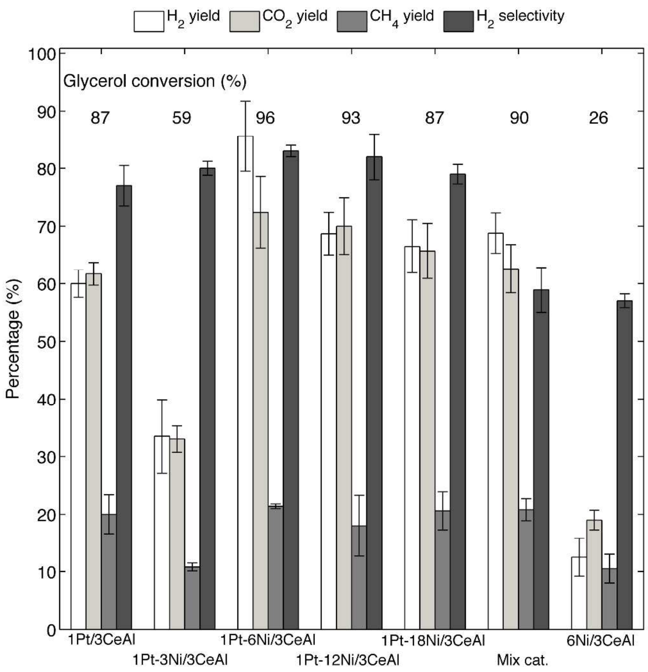

**Figure 4** Effect of adding Ni to Pt/3CeAl catalysts on yields, selectivity and glycerol conversions in the aqueous phase reforming of glycerol (240 °C, 40 bar, 1 wt% glycerol, 0.05 mL $min^{-1}$, 250 mg catalyst; data are mean values over $t$ = 5–20 h). Error bars indicate one standard deviation; each bar is the average of ≥2 experiments. Mix cat. = mixture of separate Pt/3CeAl and Ni/3CeAl catalysts with a total of 1 wt% Pt and 6 wt% Ni.

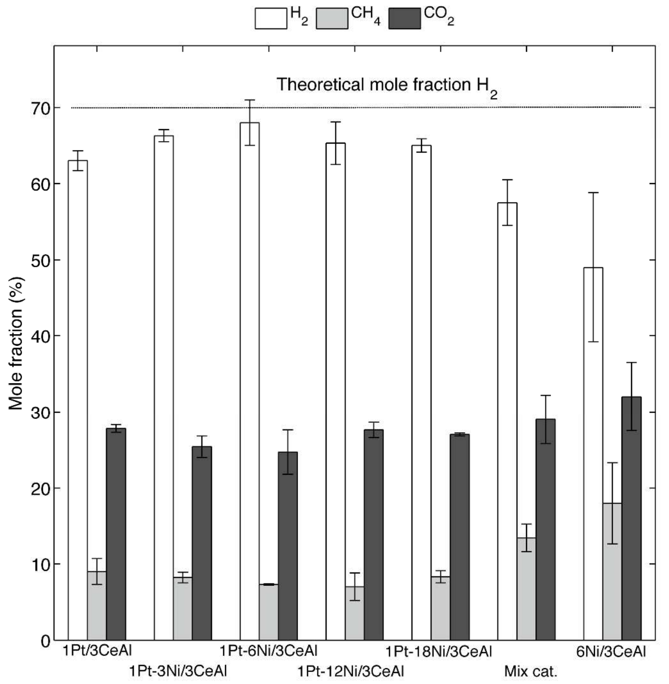

**Figure 5**. Effect of Ni addition to Pt/3CeAl catalysts on the distribution of gaseous products from the aqueous phase reforming of glycerol (240 °C, 40 bar, 1 wt% glycerol, 0.05 mL $min^{-1}$, 250 mg catalyst; data are mean values over $t$ = 5–20 h). Error bars indicate one standard deviation; each bar is the average of ≥2 experiments. Mix cat. = mixture of separate Pt/3CeAl and Ni/3CeAl catalysts with a total of 1 wt% Pt and 6 wt% Ni.

consistent with the higher activity of Ni as a WGS (Eq. 2) catalyst,[43] and may help to explain why similar $H_2$ yields were generated by these 1Pt-xNi/3CeAl catalysts and by 3Pt/3CeAl, despite the much lower Pt content of the bimetallic catalysts. However, the increased WGS activity that was provided upon Ni addition was not sufficient to explain the high $H_2$ yield and selectivity of the best catalyst, 1Pt-6Ni/3CeAl, as a mixture of separate Pt/3CeAl and Ni/3CeAl catalysts with a total of 1 wt% Pt and 6 wt% Ni did not perform as well. Despite that Ni also favors methanation,[44] the APR of glycerol over 1Pt-6Ni/3CeAl, 1Pt-12Ni/3CeAl and 1Pt-18Ni/3CeAl showed similar $CH_4$ yields to the reaction over 1Pt/3CeAl (which gave a $CH_4$ yield of 20%). This could be due to an interaction between Pt and Ni; an interaction between Pt and Cu has been credited for lowering methane production in the APR of glycerol over catalysts supported on magnesium/aluminium oxides.[40] Nevertheless, the highest fraction of $CH_4$ in the gas product (32%) was obtained using 6Ni/3CeAl as the catalyst (Figure 5).

Some authors have correlated the activity and $H_2$ selectivity of supported-metal APR catalysts with metal particle size and dispersion. Wawrzetz et al.[45] showed that $H_2$ formation from the APR of glycerol decreased with increasing Pt particle size. On the other hand, Lehnert and Claus[41] showed that bigger Pt particles produced higher $H_2$ selectivity (but similar activity), and concluded that the adsorption of glycerol occurred preferentially at face positions of the metal crystallite. Iriondo et al.[46] observed that less-dispersed Ni and PtNi catalysts were more active for the APR of glycerol. In our case, the 1Pt-6Ni/3CeAl catalyst, which had the smallest Pt metal particles (4.6 nm) and highest dispersion (25%), showed the highest $H_2$ selectivity (83%) and yield (86%).

The liquid phase from the reaction over each of the catalysts was also analyzed in order to examine the formation of larger byproducts. Apart from unreacted glycerol, we identified traces of other compounds, particularly ethanol, propylene glycol, and acetic acid. These were not quantified. The APR of 1 wt% glycerol over catalysts 1Pt-6Ni/3CeAl, 1Pt-12Ni/3CeAl and 1Pt-18Ni/3CeAl produced similar conversions and gas phase carbon yields as that over 3Pt/3CeAl, though both quantities decreased as the Ni content increased from 6 to 18 wt%.

In order to evaluate the activity and efficiency of each catalyst, the rates of $H_2$ formation were normalized to the mass of catalyst or Pt used (Figure 6). Catalysts 3Pt/3CeAl and 1Pt-6Ni/3CeAl produced almost the same amount of $H_2$ per gram of catalyst per hour, despite that the latter contained less Pt. Thus the amount of expensive metal could be reduced threefold by adding Ni, and with a slight *improvement* in $H_2$ production. Conversely, 1Pt/3CeAl and 1Pt-6Ni/3CeAl contained the same amount of Pt, but the latter produced $H_2$ approximately twice as quickly. Overall, 1Pt-6Ni/3CeAl combined the highest glycerol conversion with the greatest rate of $H_2$ production and $H_2$ selectivity, which could make it competitive for large-scale $H_2$ production.

Based upon the characterization and catalytic data, a few inferences can be drawn regarding the mechanism(s) by which

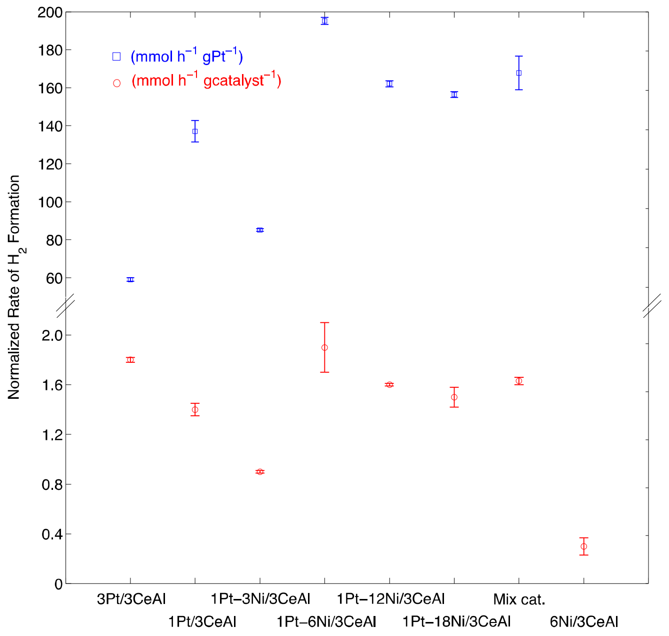

**Figure 6**. Rate of $H_2$ production from the APR of glycerol (240 °C, 40 bar, 1 wt% glycerol, 0.05 mL $min^{-1}$, 250 mg catalyst; data are mean values over $t$ = 5–20 h), normalized to the mass of catalyst or Pt used. Error bars indicate one standard deviation; each data point is the average of ≥2 experiments. Mix cat. = mixture of separate Pt/3CeAl and Ni/3CeAl catalysts with a total of 1 wt% Pt and 6 wt% Ni.

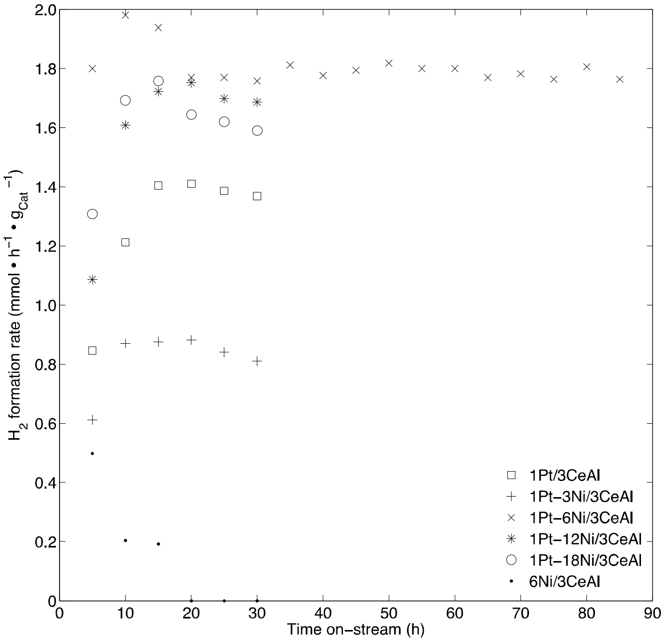

**Figure 7.** Variation of $H_2$ formation rate with time on-stream in the APR of glycerol (240 °C, 40 bar, 1 wt% glycerol, 0.05 mL min$^{-1}$, 250 mg catalyst). Each value is the average of ≥2 experiments. The best catalyst, 1Pt-6Ni/3CeAl, was tested in an extended run.

the addition of 6 wt% Ni enhanced catalyst activity. First, Ni itself contributed to the $H_2$ yield by catalyzing the WGS reaction; however, this was insufficient to explain the exceptional activity of 1Pt-6Ni/3CeAl (see above). Further, 1Pt-6Ni/3CeAl bore the smallest and most-dispersed Pt nanoparticles, and thus had more Pt atoms located at the particle surfaces than the Ni-free catalyst with the same Pt loading. Shabaker et al. have also noted a correlation between Pt dispersion and the apparent activation energy in APR, albeit on a range of different supports.[6] Finally, the XRD pattern and X-ray photoelectron spectrum of 1Pt-6Ni/3CeAl pointed to interactions between Pt and Ni (see above), including the dissolution of some Ni atoms in the Pt (i.e. surface, though not bulk, alloy formation); both computational[35] and experimental[36, 37] studies have demonstrated that surface Pt-Ni alloys bind $H_2$ less strongly than Pt$^0$. The importance of $H_2$ binding strength has been demonstrated by Shabaker et al.,[47] who showed that hydrogen inhibits the APR of oxygenated hydrocarbons on Pt catalysts, likely by occupying and thus blocking Pt active sites. Similarly, Huber et al.[5] speculated that supported Pt-Ni and Pt-Co catalysts, which outperformed a supported Pt catalyst, had lower heats of $H_2$ and CO adsorption than pure Pt, and thus more unoccupied active sites accessible to reactants. Thus the exceptional activity of 1Pt-6Ni/3CeAl

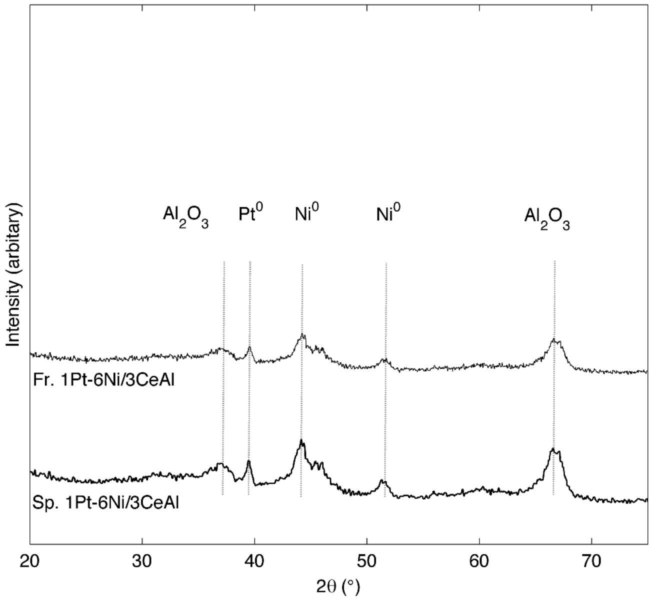

**Figure 8**. XRD patterns of 1Pt-6Ni/3CeAl catalyst freshly reduced in flowing $H_2$ (50 vol% in $N_2$) at 800 °C for 60 min, and spent after 30 h on-stream (240 °C, 40 bar, 1 wt% glycerol, 0.05 mL min$^{-1}$, 250 mg catalyst).

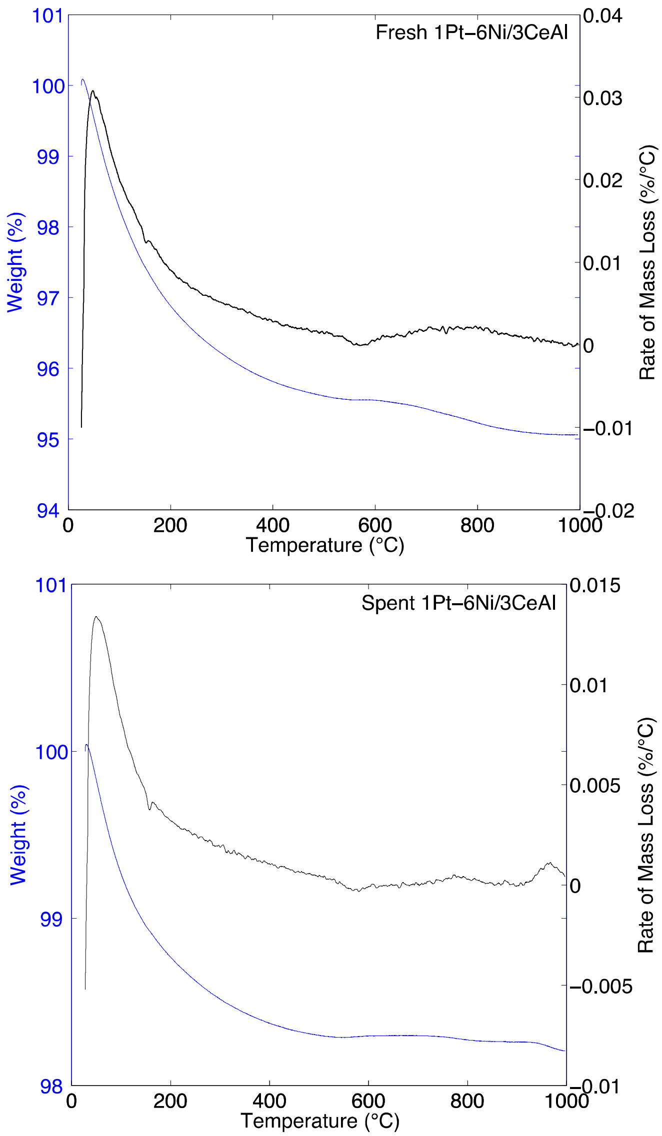

**Figure 9.** Thermogravimetric analysis of fresh (reduced: 50 vol% $H_2$ in $N_2$, 800 °C, 60 min) and spent (after reaction: 240 °C, 40 bar, 1 wt% glycerol, 0.05 mL min$^{-1}$, 85 h) 1Pt-6Ni/3CeAl. Samples were heated at 10 °C min$^{-1}$ in instrument air (40 vol% in $N_2$).

was likely caused by a confluence of factors; in particular, it offered the best balance of advantageous Ni–Pt interactions and high Pt dispersion/small Pt particle size.

One of the major problems related to the operation of heterogeneous catalysis is the loss of catalytic activity, i.e. "deactivation", over time, and Ni catalysts are generally more susceptible than noble-metal catalysts. Figure 7 shows the stability of our ceria–alumina-supported catalysts in the APR of glycerol over 30 h on-stream. Only catalyst 6Ni/3CeAl was severely deactivated; it ceased to produce a detectable $H_2$ peak after 15 h on-stream. In a longer test, $H_2$ formation over the most active catalyst, 1Pt-6Ni/3CeAl, occurred at a relatively constant rate over 85 h.

Two main causes of catalyst deactivation in APR are carbon deposition and the sintering of the active metal,[12] and we therefore examined the catalysts for signs of these problems. Figure 8 presents the XRD patterns of the fresh and spent 1Pt-6Ni/3CeAl catalysts; patterns for the remaining catalysts are shown in Figure S11. No carbon formation[48] (expected at 2θ = 25.5°) or NiO (2θ = 37.2 and 62.9°)[25] was observed on the spent 1Pt-6Ni/3CeAl catalyst after 85 h on-stream. Rather, the only difference observed was in the widths of the $Pt^0$ and $Ni^0$ peaks, which were slightly sharper in the XRD pattern of spent 1Pt-6Ni/3CeAl. This could have indicated a small amount of particle agglomeration (based upon the Pt (111) peak, calculated particle sizes were 4.6 and 4.7 nm, respectively, for the fresh and spent catalysts). The X-ray photoelectron spectrum of spent 1Pt-6Ni/3CeAl showed a signal for the Pt $4f_{7/2}$ electrons (Figure S14a) that was similar to the one for the fresh catalyst, though with a slightly higher energy ($BE_{Pt\ 4f(7/2)}$ = 71.45 eV). This energy shift could have been due to increased interaction with Ni; however, because of its small magnitude ($\Delta BE_{Pt\ 4f(7/2)}$ = 0.1 eV), the effects of charge compensation cannot be ruled out. The Ni $2p_{3/2}$ signals of the fresh and spent catalysts (Figure S14b) were also similar, though the latter showed higher relative intensity at lower binding energy. This would seem to indicate that the $Ni^0/Ni^{2+}$ ratio was greater on the surface of the spent than the fresh catalyst; however, as both catalysts were exposed to air prior to measurement, and as Ni surfaces can be oxidised in air, conclusions based upon this comparison would be dubious. Nevertheless, consistent with the XRD results, the spent catalyst clearly bore $Ni^0$. The liquid products of the APR of glycerol over 1Pt-6Ni/3CeAl were analysed for metal content using inductively coupled plasma/mass spectrometry (ICP–MS). A small amount (<1 ppm) of Ni was present, representing a loss of <0.001% of the Ni in the catalyst, but no Pt could be detected. The XPS analysis of spent 1Pt-6Ni/3CeAl also indicated that its surface contained significantly less carbon than the fresh catalyst (1.8 vs. 8.1 at% based on detection-sensitivity-corrected areas; see Figure S13); thus adventitious carbon was likely the main source of surface carbon. Finally, as amorphous carbon deposition would not have been seen in the XRD pattern, we also performed a thermogravimetric analysis (TGA) of spent 1Pt-6Ni/3CeAl in air (Figure 9). No evidence of weight loss due to carbon combustion was observed, supporting the idea that no significant carbon deposition occurred on 1Pt-6Ni/3CeAl.

On the other hand, the TGA of 6Ni/3CeAl after a 30-h use (shown, along with TGA curves for the other spent catalysts, in Figure S12) revealed that combustible material, presumably carbon (greatest weight loss occurred over T = 500–600 °C), made up >4 wt% of the sample, and the XPS scan showed that the surface of spent 6Ni/3CeAl bore twice as much C as the fresh catalyst. NiO peaks were clearly observed in the XRD of spent 6Ni/3CeAl (Figure S11), and neither XRD nor XPS (Figure S14b) showed evidence of $Ni^0$ in that sample. Thus both modes of catalyst inactivation, i.e. metal oxidation and carbon deposition, contributed to the failure of 6Ni/3CeAl after only 15 h on-stream. Moreover, ICP–MS analysis of the liquid products evinced significant nickel loss (1300 ppm, representing 0.8% of the Ni metal in the catalyst) from 6Ni/3CeAl following 30 h on-stream. The spent sample of a catalyst with intermediate stability, 1Pt-18Ni/3CeAl, was also studied. No evidence of NiO formation was observed in the XRD pattern of that catalyst (Figure S11), the Ni $2p_{3/2}$ signals in the XPS of the fresh and spent samples were virtually identical (Figure S14b), and the losses of Ni and Pt to solution were below the limits of detection. However, the spent sample did lose mass upon combustion (Figure S12), indicating that although metal oxidation was not a significant problem, some carbon was deposited on that catalyst, and was presumably responsible for the minor decline in its activity after 20 h on-stream (Figure 7).

## Conclusion

We have previously shown that a 3Pt/3CeAl catalyst was more active and more selective towards $H_2$ production than $3Pt/Al_2O_3$ in the APR of glycerol.[11] Pt catalysts are highly active for APR, but Pt is expensive, making catalysts containing little or no Pt desirable. Bimetallic Pt-Ni catalysts active for the APR of glycerol to $H_2$ were developed in this work. Bimetallic 1Pt-6Ni/3CeAl showed the highest $H_2$ yield and gas phase C yield, and produced three times as much $H_2$ per gram of Pt as 3Pt/3CeAl. The favourable characteristics of 1Pt-6Ni/3CeAl could not be attributed to a single factor, but rather appeared to stem from smaller crystallite size (4.6 nm), higher metal dispersion (25%) and greater degree of electronic interaction ($BE_{Pt\ 4f(7/2)}$ = 71.35 eV) between the metals, likely as surface alloy formation. Further, the 3-wt%-$CeO_2$-doped $Al_2O_3$ support enhanced both the activity and selectivity towards $H_2$ production. As a result 1Pt/3CeAl showed higher glycerol conversion and $H_2$ yield than the benchmark catalyst, $3Pt/Al_2O_3$.[11] Future work will study APR over 1Pt-6Ni/3CeAl at higher glycerol concentrations and on larger scales.

## Experimental Section

### Catalyst preparation

The 3-wt% $CeO_2$–$Al_2O_3$ supports were prepared by impregnating 2.0 g of dried (120 °C overnight) γ-$Al_2O_3$

(Sigma–Aldrich) with a solution prepared by dissolving 197 mg of $(NH_4)_2[Ce(NO_3)_6]$ (99%, Sigma–Aldrich) in 10 mL deionized water in a 100-mL glass vial. The mixture was stirred overnight at room temperature, and the water was allowed to evaporate. The sample was then dried in air at 120 °C for 12 h and calcined under flowing air at 600 °C for 3 h (heating rate 1.5 °C $min^{-1}$). $[Pt(NH_3)_4](NO_3)_2$ (Strem Chemical) and $Ni(NO_3)_2 \bullet 6H_2O$ (Sigma–Aldrich) were dissolved, individually or together, into a minimum amount of deionized water to make monometallic or bimetallic catalysts, respectively. These were deposited on 3-wt% $CeO_2–Al_2O_3$ supports (3CeAl) using a conventional impregnation technique. Specifically, to prepare 1Pt-3Ni/3CeAl, 2.205 g of calcined $3CeO_2–Al_2O_3$ support was impregnated with a solution prepared by dissolving 43.1 mg $[Pt(NH_3)_4](NO_3)_2$ and 324.5 mg of $Ni(NO_3)_2 \bullet 6H_2O$ in 10 mL of deionized water in a 100-mL glass vial. The mixture was then stirred overnight at room temperature, and the water was allowed to evaporate. The sample was then dried in air at 120 °C for 12 h and calcined under flowing air at 600 °C for 6 h (heating rate 1.5 °C $min^{-1}$). Catalysts were reduced ex situ in flowing hydrogen (50 mL $min^{-1}$) at 800 °C for 60 min (heating rate 1.5 °C $min^{-1}$) at atmospheric pressure and stored under vacuum prior to use. For comparison, a mixed "1Pt/3CeAl + 6Ni/3CeAl" catalyst was also prepared. In order to prepare this physical mixture of catalysts with a total of 1 wt% Pt and 6 wt% Ni, catalysts 2Pt/3CeAl and 12Ni/3CeAl were independently prepared, then mixed in a 1:1 ratio by mass; this was noted as "Mix cat."

### Catalyst characterization

The textural properties of the catalysts were measured by $N_2$ adsorption-desorption at liquid nitrogen temperature (−196 °C) using an Autosorb-iQ apparatus (Quantachrome). Prior to analysis, the samples were outgassed for 12 h at 140 °C. The specific surface areas were determined from the linear portions of the adsorption isotherms ($P/P_0 = 0.05–0.35$) using the Brunauer–Emmett–Teller method,[21] and the pore volumes were calculated at $P/P_0 = 0.995$. The pore-size distributions were calculated from the adsorption isotherms using the Barrett–Joyner–Halenda (BJH) formula.[22] Isotherms are displayed in the Supporting Information (Figure S1). The crystalline structures of the supported catalysts were determined by X-ray diffractometry using Cu Kα radiation (λ = 0.1542 nm) and a graphite monochromator (Shimadzu S6000). The instrument was operated at 40 kV and 40 mA. Scans were recorded over the range 2θ = 10–75° in steps of 0.01°, and data for each point was collected for 1 s. The mean Pt crystallite sizes were calculated by applying the Scherrer equation[23] to the Pt (111) peak, and the corresponding Pt (or Pt-Ni) dispersion, $M_{disp}$, was estimated according to Eq. 5:[24]

$$M_{disp} = 6V/dA \tag{5}$$

Here, V is the Pt atomic volume (0.0151 $nm^3$), d is the crystallite size (nm) and A is the surface area of a single Pt atom (0.080 $nm^2$). Scanning electron microscopy (FESEM, Zeiss Ultra+) was used to examine the morphology of fresh and spent catalysts (Figure S2) and transmission electron microscopy (TEM, Philips CM120 BioFilter) was employed to gain insight into the inner pore structure and the distribution of metal sites (Figure S3). X-ray photoelectron spectra were recorded on an ESCALAB250Xi (Thermo Scientific, UK) using a monochromated Al Kα source (1486.68 eV) operating at 164 W (10.8 mA and 15.2 kV) and under a vacuum of ≤2 × $10^{-9}$ mbar. Binding energies were referenced to the adventitious hydrocarbon C 1*s* signal at 285.0 eV. For spent samples, the binding energies were adjusted to give the same Al 2*p* binding energy as in the corresponding fresh samples. The Ce 3*d* and Pt $4d_{5/2}$ regions of the XPS spectra are shown in Figures S9 and S10, respectively. Note that the characterisation of reduced catalysts occurred ex situ (see "Catalyst Preparation"); therefore, materials were exposed to ambient conditions prior to and, in the case of XRD, during data collection. Thermogravimetric analysis of the spent catalysts was measured on a TA Instruments Q500 analyser under a flow of 40 mL $min^{-1}$ instrument air. Samples were heated at 10 °C $min^{-1}$ to 1000 °C.

### Catalytic test

The APR of glycerol was studied in a continuous-flow fixed-bed reactor system. The catalyst (250 mg) was loaded into a 5-mm i.d. stainless steel tubular reactor and held in position with quartz wool plugs. Reaction temperature was measured by a K-type thermocouple that was placed inside the reactor, very close to the catalyst bed. The reactor was mounted in a tube furnace (MTI GSL-1100X). A backpressure regulator (0 to 68 bar, Swagelok) attached to a pressure gauge was used to pressurize the system with $N_2$ to 40 bar. A schematic of the reactor can be found in Figure S4. A 1-wt% glycerol solution was introduced using a digital hplc pump (Waters 510) at a rate of 0.05 mL $min^{-1}$, and heating of the catalyst bed was initiated. When the reactor reached 240 °C, $N_2$ flow was set at 50 sccm using a Bronkhorst mass flow controller. The system was allowed to stabilize for about 2 h before analysis of the reaction products began.

Gas products were analyzed at 25-min intervals using an online gas chromatograph (Varian CP-3800) equipped with one Hayesep N, 60/80 Mesh, 5 m × 1/8″ SST column and one Molsieve 5Å, 60/80 Mesh, 1 m × 1/8" column, connected in series. Thermal conductivity (TCD) and flame ionization (FID) detectors, in series, were used to analyze $H_2$ and hydrocarbons, respectively. The GC was calibrated using highly pure gases (grade 5.0) from Coregas. For each reading, ten successive injections were made and the relative standard deviations were measured. The calibration curves (Figure S5) were developed, and the samples were analyzed, with the oven at 80 °C, the TCD at 200 °C and the FID at 300 °C. A representative GC curve (Figure S6) shows only four peaks, representing $H_2$, $N_2$, $CH_4$ and $CO_2$, respectively, for each injection of product gas.

The liquid products of the APR reaction were collected in a condenser downstream of the reactor bed (refer to Figure S4), and aliquots of the condensed liquid were analyzed with a Shimadzu HPLC, comprising a degasser (DGU-20A5), a pump

(LC-20AD), an autosampler (SIL-20A HT), an oven (CTO-20A), and a refractive index detector (RID-10A). A Rezex RCM-Monosaccharide column (300 × 7.8 mm) was used for analyte separation. Ultrapure DI water (flow rate 0.5 mL min$^{-1}$) was used as the eluent. A representative HPLC trace and a calibration curve for glycerol are shown in Figure S7. As the intercept of the calibration curve was non-zero, glycerol concentration will be overestimated when the conversion is high, and thus conversion will be underestimated under those circumstances. The catalysts were evaluated on the bases of $H_2$, $CO_2$ and $CH_4$ yield, as well as carbon conversion to gas, $H_2$ selectivity and glycerol conversion efficiency. These were calculated according to:

$$\text{Yield of species } x = \frac{\text{moles of } x \text{ produced experimentally}}{\text{moles of } x \text{ produced theoretically}} \text{ x } 100\%$$

$$\text{C conversion to gas} = \frac{\text{moles of C in the gas products}}{\text{moles of C fed into the reactor}} \text{ x } 100\%$$

$$H_2 \text{ selectivity} = \frac{2 \text{ x moles of } H_2 \text{ produced experimentally}}{\text{Total H atoms in the gas products}} \text{ x } 100\%$$

$$\begin{matrix}\text{Glycerol}\\ \text{conversion}\end{matrix} = \left[1 - \frac{\text{moles of glycerol in liquid products}}{\text{moles of glycerol in feed}}\right] \text{ x } 100\%$$

## Acknowledgements

M.M.R is grateful to the University of Sydney for a postgraduate scholarship. The authors are grateful to the Australian Centre for Microscopy & Microanalysis (ACMM) at the University of Sydney for SEM and TEM facilities and to Mr. V. Lo for his assistance with SEM and TEM analysis, to Dr. B. Gong from the University of New South Wales Surface Analytical Centre for his assistance with XPS analysis, to Ms. D. Yu from the University of New South Wales for assistance with ICP–MS, and to Dr. J. Shi from the School of Chemical and Biomolecular Engineering, University of Sydney, for assistance with $N_2$ adsorption measurements.

## Notes and references

[a] School of Chemical and Bio-molecular Engineering, University of Sydney, Sydney, NSW, 2006, Australia. E-mail: mrah7493@uni.sydney.edu.au (M.M.R), Andrew.minett@sydney.edu.au (A.I.M)

1. B. C. R. Ewan and R. W. K. Allen, *Int. J. Hydrogen Energy*, 2005, 30, 809-819.
2. S. Dunn, *Int. J. Hydrogen Energy*, 2002, 27, 235-264.
3. R. D. Cortright, R. R. Davda and J. A. Dumesic, *Nature*, 2002, 418, 964-967.
4. G. W. Huber, R. D. Cortright and J. A. Dumesic, *Angew. Chem. Int. Ed.*, 2004, 43, 1549-1551.
5. G. W. Huber, J. W. Shabaker, S. T. Evans and J. A. Dumesic, *Applied Catalysis B: Environmental*, 2006, 62, 226-235.
6. J. W. Shabaker, G. W. Huber, R. R. Davda, R. D. Cortright and J. A. Dumesic, *Catal. Lett.*, 2003, 88, 1-8.
7. S. Adhikari, S. D. Fernando and A. Haryanto, *Renewable Energy*, 2008, 33, 1097-1100.
8. R. R. Soares, D. A. Simonetti and J. A. Dumesic, *Angew. Chem. Int. Ed.*, 2006, 45, 3982-3985.
9. R. R. Davda, J. W. Shabaker, G. W. Huber, R. D. Cortright and J. A. Dumesic, *Applied Catalysis B: Environmental*, 2005, 56, 171-186.
10. R. R. Davda, J. W. Shabaker, G. W. Huber, R. D. Cortright and J. A. Dumesic, *Applied Catalysis B: Environmental*, 2003, 43, 13-26.
11. M. M. Rahman, T. L. Church, A. I. Minett and A. T. Harris, *ChemSusChem*, 2013, 6, 1006-1013.
12. J. W. Shabaker, G. W. Huber and J. A. Dumesic, *J. Catal.*, 2004, 222, 180-191.
13. C. Crisafulli, S. Scirè, S. Minicò and L. Solarino, *Applied Catalysis A: General*, 2002, 225, 1-9.
14. R. N. Widyaningrum, T. L. Church and A. T. Harris, *Catal. Commun.*, 2013, 35, 45-50.
15. R. T. K. Baker, J. A. Dumesic and J. J. Chludzinski Jr, *J. Catal.*, 1986, 101, 169-177.
16. E. L. Kunkes, D. A. Simonetti, J. A. Dumesic, W. D. Pyrz, L. E. Murillo, J. G. Chen and D. J. Buttrey, *J. Catal.*, 2008, 260, 164-177.
17. X. Wang, N. Li, L. D. Pfefferle and G. L. Haller, *Catal. Today*, 2009, 146, 160-165.
18. R. L. Manfro, T. P. M. D. Pires, N. F. P. Ribeiro and M. M. V. M. Souza, *Catalysis Science & Technology*, 2013, 3, 1278-1287.
19. E.-Y. Ko, E. Park, K. Seo, H. Lee, D. Lee and S. Kim, *Catal. Lett.*, 2006, 110, 275-279.
20. S. A. Tupy, A. M. Karim, C. Bagia, W. Deng, Y. Huang, D. G. Vlachos and J. G. Chen, *ACS Catalysis*, 2012, 2, 2290-2296.
21. S. Brunauer, P. H. Emmett and E. Teller, *J. Am. Chem. Soc.*, 1938, 60, 309-319.
22. E. P. Barrett, L. G. Joyner and P. P. Halenda, *J. Am. Chem. Soc.*, 1951, 73, 373-380.
23. A. Guiner, *X-ray Diffraction in Crystals, Imperfect Crystals and Amorphous Bodies, Dover Publications Inc., New York*, 1994.
24. J. R. Anderson, *Structure of Metallic Catalysts, Academic Press Inc., London*, 1975.
25. A. Iriondo, V. L. Barrio, J. F. Cambra, P. L. Arias, M. B. Güemez, R. M. Navarro, M. C. Sánchez-Sánchez and J. L. G. Fierro, *Top. Catal.*, 2008, 49, 46-58.
26. R. L. Manfro, A. F. da Costa, N. F. P. Ribeiro and M. M. V. M. Souza, *Fuel Process. Technol.*, 2011, 92, 330-335.
27. P. C. Sherrell, W. Zhang, J. Zhao, G. G. Wallace, J. Chen and A. I. Minett, *ChemSusChem*, 2012, 5, 1233-1240.
28. G. Wen, Y. Xu, Z. Xu and Z. Tian, *Catal. Lett.*, 2009, 129, 250-257.
29. S. Damyanova and J. M. C. Bueno, *Applied Catalysis A: General*, 2003, 253, 135-150.
30. A. Tegou, S. Papadimitriou, I. Mintsouli, S. Armyanov, E. Valova, G. Kokkinidis and S. Sotiropoulos, *Catal. Today*, 2011, 170, 126-133.
31. X.-Z. Fu, Y. Liang, S.-P. Chen, J.-D. Lin and D.-W. Liao, *Catal. Commun.*, 2009, 10, 1893-1897.
32. P. Nash and M. F. Singleton, *Bulletin of Alloy Phase Diagrams*, 1989, 10, 258-262.

33. U. Esch and A. Schneider, *Zeitschrift für Elektrochemie und angewandte physikalische Chemie*, 1944, 50, 268-274.
34. K.-W. Park, J.-H. Choi, B.-K. Kwon, S.-A. Lee, Y.-E. Sung, H.-Y. Ha, S.-A. Hong, H. Kim and A. Wieckowski, *The Journal of Physical Chemistry B*, 2002, 106, 1869-1877.
35. J. Greeley, Mavrikakis, M., *Nat Mater*, 2004, 3, 810-815.
36. B. Frühberger, J. Eng, Jr. and J. G. Chen, *Catal. Lett.*, 1997, 45, 85-92.
37. H. H. Hwu, J. Eng and J. G. Chen, *J. Am. Chem. Soc.*, 2002, 124, 702-709.
38. D. Zhao and B.-Q. Xu, *Angew. Chem. Int. Ed.*, 2006, 45, 4955-4959.
39. A. P. Grosvenor, M. C. Biesinger, R. S. C. Smart and N. S. McIntyre, *Surf. Sci.*, 2006, 600, 1771-1779.
40. D. A. Boga, R. Oord, A. M. Beale, Y.-M. Chung, P. C. A. Bruijnincx and B. M. Weckhuysen, *ChemCatChem*, 2013, 5, 529-537.
41. K. Lehnert and P. Claus, *Catal. Commun.*, 2008, 9, 2543-2546.
42. D. L. King, L. Zhang, G. Xia, A. M. Karim, D. J. Heldebrant, X. Wang, T. Peterson and Y. Wang, *Applied Catalysis B: Environmental*, 2010, 99, 206-213.
43. D. C. Grenoble, M. M. Estadt and D. F. Ollis, *J. Catal.*, 1981, 67, 90-102.
44. M. A. Vannice, *J. Catal.*, 1977, 50, 228-236.
45. A. Wawrzetz, B. Peng, A. Hrabar, A. Jentys, A. A. Lemonidou and J. A. Lercher, *J. Catal.*, 2010, 269, 411-420.
46. A. Iriondo, J. F. Cambra, V. L. Barrio, M. B. Guemez, P. L. Arias, M. C. Sanchez-Sanchez, R. M. Navarro and J. L. G. Fierro, *Applied Catalysis B: Environmental*, 2011, 106, 83-93.
47. J. W. Shabaker, R. R. Davda, G. W. Huber, R. D. Cortright and J. A. Dumesic, *J. Catal.*, 2003, 215, 344-352.
48. J. Comas, F. Mariño, M. Laborde and N. Amadeo, *Chem. Eng. J.*, 2004, 98, 61-68.